

Flat-band ratio and quantum metric in the superconductivity of modified Lieb lattices

Reko P. S. Penttilä,¹ Kukka-Emilia Huhtinen,^{1,2} and Päivi Törmä^{1,*}

¹*Department of Applied Physics, Aalto University School of Science, FI-00076 Aalto, Finland*

²*Institute for Theoretical Physics, ETH Zurich, CH-8093, Switzerland*

Flat bands may offer a route to high critical temperatures of superconductivity. It has been predicted that the quantum geometry of the bands as well as the ratio of the number of flat bands to the number of orbitals determine flat band superconductivity. However, such results have assumed at least one of the following: an isolated flat band, zero temperature, mean-field theory, and/or uniform pairing. Here, we explore flat band superconductivity when these assumptions are relaxed. We consider an attractive Hubbard model for different extensions of the Lieb lattice. The superconducting order parameter, critical temperature, superfluid weight, and Berezinskii-Kosterlitz-Thouless temperature are calculated within dynamical mean-field theory. We find that while the flat-band ratio and quantum geometry are good indicators of superconductivity near zero temperature, at finite temperatures the behavior is more complicated. Our results suggest that the properties of the other bands near the flat band(s) are crucial.

I. INTRODUCTION

Both theory and experiments suggest that flat bands can be beneficial for superconductivity. Studies of superconductivity on twisted bilayer graphene, a material with (nearly) flat bands at certain twist angles, have shown one of the highest T_c to charge carrier density ratios ever measured.^{1–5} On the theory side, even the simple Bardeen-Cooper-Schrieffer (BCS) theory predicts that the critical temperature for flat bands is proportional to the effective attractive interaction $|U|$,^{6,7} while the critical temperature for dispersive bands is given by $T_c \propto \exp(-1/|U|\rho_0)$, where ρ_0 is the density of states at the Fermi surface. This indicates that T_c could be greatly enhanced in flat bands.

Furthermore, it has been theoretically shown that flat bands can have a non-zero superfluid weight and thus support dissipationless transport,⁸ which is not immediately clear since non-interacting flat-band states are localized. In an isolated perfectly flat band, the superfluid weight (stiffness) D_s is completely of quantum geometric origin, i.e. a non-zero quantum metric,⁹ Berry curvature or Chern number enables supercurrent.^{8,10–12} It has also been shown that the superfluid weight at zero temperature, for flat bands isolated from other bands by a gap larger than the interaction scale $|U|$ (“isolated flat bands”) and fulfilling the so-called uniform pairing condition¹³ which requires the order parameters to be equal at all orbitals where the flat band states reside, is proportional to the minimal quantum metric^{8,14} and to the ratio of the number of degenerate flat bands to orbitals where the flat band states reside (“flat-band ratio”).¹⁵ These results have been derived both within mean-field theory^{8,14} and by exact calculations at zero temperature^{14,15} — always assuming the isolated flat band and uniform pairing conditions.

In the search of new superconducting materials with high critical temperatures and other desirable properties such as high critical currents, efficient rules of thumb as well as relations between superconductivity and simple band structure properties (quantum geometry, number of flat bands), would be immensely useful. It is therefore of interest to explore whether the existing simple relations hold beyond

the restrictive conditions for which they have been derived. The analytical prediction that the flat band superfluid weight and critical temperature is linearly proportional to the interaction, $D_s \propto |U|$, derived by mean-field for isolated flat bands,⁸ has been verified by various numerical methods including quantum Monte Carlo, density matrix renormalization group and dynamical mean-field (DMFT) calculations.^{16–23} There exist also a few studies on how to describe the case of flat bands touching other bands,^{24–26} within mean-field or effective theories. For some lattice models, expressions have also been obtained for the zero-temperature mean-field superfluid weight in flat bands not fulfilling the uniform pairing condition.¹⁹ Systematic finite-temperature, beyond-mean-field studies of the validity of the relations between the superfluid weight and the quantum metric, as well as the flat-band ratio, are missing. The goal of this article is to take the first steps in this direction.

We chose as our model system various extensions of the Lieb lattice, since this will allow us to systematically change the number of flat bands and the quantum geometry. The calculations of the superconducting order parameter and the superfluid weight are done using DMFT, as it can describe the local (in our case within the unit cell) quantum and thermal fluctuations exactly. We show by comparison to a mean-field calculation that such a beyond mean-field approach is necessary.

In Section II A, we present the different lattice models studied in this work and provide the Hamiltonian used. In section II, we present the results of the DMFT calculations. We show that the quantum metric and the flat-band ratio can be good predictors of superconductivity at zero or very low temperatures, even if the system is not in the isolated flat band and uniform pairing limit. However, while they still give some guidelines at finite temperatures, the behavior is more complex, indicating that the properties of the nearby bands play an important role.

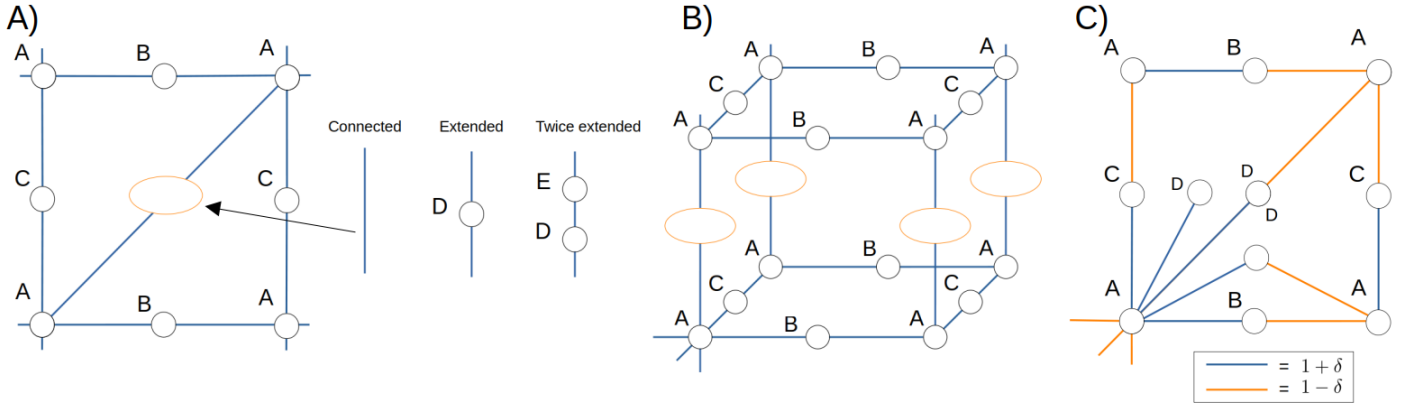


Figure 1. a) Different two-dimensional extensions of the Lieb lattice called connected, extended and twice-extended. b) Different three-dimensional extensions. c) Different versions of the two-dimensional extended Lieb lattice.

II. RESULTS

A. The system

In this study, we investigate different extensions of the Lieb lattice in two and three dimensions. The two-dimensional Lieb lattice is a bipartite lattice (see Fig.1 a) without the diagonal line from site A to another site A) featuring a single zero-energy flat band. Its extensions allow us to change the number of flat bands and tune the quantum metric of the lattice. Fig.1 a) shows three different extensions in two dimensions, all constructed by connecting the next nearest A sites with either a straight hopping term or additional orbitals. We name the different extensions in the following way: the straight hopping connection is the connected Lieb lattice, one additional orbital is the extended Lieb lattice and the extension with two additional orbitals is the twice-extended Lieb lattice. The blue lines give the allowed hoppings with a hopping energy of $t = 1$. All energies and temperatures in this article are given in units of the hopping t , and we set the Planck's and Boltzmann constants and the electron charge to unity, $\hbar = k_B = e = 1$.

Fig.1 b) shows different three-dimensional extensions of the Lieb lattice, which are constructed by stacking two-dimensional Lieb lattices and connecting them from the A sites with either a direct hopping connection or with additional orbitals. The three-dimensional extensions are named similarly to the two-dimensional extensions. All of these extensions in both two and three dimensions preserve the original zero-energy flat band of the Lieb lattice since the localized flat-band states in the Lieb lattice reside only on the B/C orbitals and we make the extensions from the A orbitals. In the Lieb, connected and twice extended lattices, there is a single flat band with states residing at the B/C orbitals. In the extended Lieb lattice, there are two flat bands with states residing at the $B/C/D$ orbitals. The ratio of the number of degenerate flat bands, N_f , to the number of orbitals at which the flat band states reside, N_{of} , called the flat-band ratio, is therefore different: in the Lieb, connected and twice extended lattices $N_f/N_{of} = 1/2$,

whereas in the extended Lieb lattices $N_f/N_{of} = 2/3$.

Fig.1 c) presents different versions of the two-dimensional extended Lieb lattice, called the diagonal, x-directional, and decorated versions. In the diagonal version, the extension is made diagonally from the A site to the A site of the next-nearest unit cell, while in the x-directional version, the extension is made to the next unit cell in the x-direction. In the decorated Lieb lattice, an additional orbital is added to the unit cell and connected only to the A orbital of the same unit cell. All of these different versions have two flat bands with states residing at three different orbitals, resulting in a flat-band ratio of $N_f/N_{of} = 2/3$. The hoppings are altered with a hopping parameter δ , which increases the hoppings inside the unit cell (blue lines) and decreases the hoppings between unit cells (orange lines). Setting $\delta \neq 0$ will allow us to open a band gap in those lattices that have a Dirac cone touching the flat band, which makes the integrated quantum metric of the flat band, used in our analysis, finite.

We study the multi-band Hubbard Hamiltonian with an attractive onsite interaction $U < 0$

$$H = \sum_{\langle n, n' \rangle} t_{n, n'} c_{n\sigma}^\dagger c_{n'\sigma} + \mu \sum_n c_{n\sigma}^\dagger c_{n\sigma} + U \sum_n c_{n\uparrow}^\dagger c_{n\uparrow} c_{n\downarrow}^\dagger c_{n\downarrow}, \quad (1)$$

where $n \equiv i, \alpha$ labels the unit cell i and the orbital α . The solutions of this Hamiltonian are given by Green's functions, with the Nambu-Gorkov formalism where, for a lattice with M orbitals in the unit cell, both the Green's functions and self-energies are $2M \times 2M$ matrices. This is essential since we have to include anomalous components that describe Cooper pairing in the system. The Green's functions and the self-energy are then given by

$$\mathbf{G}_i(i\omega_n) = \begin{bmatrix} G_i(i\omega_n) & F_i(i\omega_n) \\ F_i^*(i\omega_n) & -G_i^*(i\omega_n) \end{bmatrix}, \quad (2)$$

$$\mathbf{\Sigma}_i(i\omega_n) = \begin{bmatrix} \Sigma_i(i\omega_n) & S_i(i\omega_n) \\ S_i^*(i\omega_n) & -\Sigma_i^*(i\omega_n) \end{bmatrix}, \quad (3)$$

where $G_i(i\omega_n)$ and $\Sigma_i(i\omega_n)$ ($F_i(i\omega_n)$ and $S_i(i\omega_n)$) are the normal (anomalous) components of the Green's function

and the self-energy, respectively. All of these components are $M \times M$ matrices. We assume the Green's functions and self-energies depend only on the relative unit cell index i because of the translational invariance of the lattice. The order parameters of each orbital can be obtained from the diagonal elements of the anomalous components of the local Green's functions, $F_{loc}(i\omega_n)$, which we calculate using dynamical mean-field theory (DMFT):

$$\Delta_\alpha = [F_{loc}(i\omega_n)]_{\alpha,\alpha}. \quad (4)$$

We also calculate the superfluid weight for the presented lattices with DMFT using linear response theory (details are presented in section IV).

B. Two-dimensional extensions

In this section, we present the results of DMFT calculations for the different two-dimensional extensions shown in Fig.1 a). The quantities of interest are the order parameters and superfluid weight as a function of temperature. Figures 2 a) and c) show the order parameters of the original Lieb lattice and two-dimensional extended Lieb lattice, respectively. The interaction strength is $|U| = 1$ and the chemical potential is $\mu = 0$, corresponding to a half-filled flat band in both of the lattices. We see that the critical temperatures of the order parameters, i.e., the temperature at which the order parameters vanish, increase from the original to the extended Lieb lattice. Moreover, the absolute values of the order parameters are larger for the extended Lieb geometry.

Figures 2 b) and d) show all the components of the superfluid weight and the square root of its determinant for the original and extended Lieb lattices, respectively. The superfluid weights become zero at the critical temperature of the order parameters of the corresponding lattices. However, the real critical temperature is given by the BKT transition temperature, which is $T_{BKT} \approx 0.51$ for the extended Lieb lattice and $T_{BKT} \approx 0.47$ for the original Lieb lattice. These results indicate that this extension of the Lieb lattice benefits superconductivity because of the larger T_{BKT} .

Next, we present the results of the same calculation for all two-dimensional extensions shown in Fig.1 a). Figure 3 a) shows $|\Delta_B|$ for these extensions and the original Lieb lattice. It is enough to look only at $|\Delta_B|$ since, even though the order parameters do not have the same amplitude at all orbitals, they vanish at the same temperature. These results are obtained from DMFT calculations with attractive interaction strength $|U| = 1$ and chemical potential $\mu = 0$. We see that while the critical temperature T_C of $|\Delta_B|$ for the extended Lieb lattice is increased from the original Lieb lattice, T_C stays approximately the same for the connected Lieb lattice.

These findings are qualitatively in line with the mean-field result $T_C \approx |U|N_f/(4N_{of})$, which shows that the critical temperature for the order parameters is approximately proportional to the flat-band ratio N_f/N_{of} . This result has been obtained assuming the uniform pairing condition and

isolated flat bands (see appendix IX C). In the Lieb and connected lattices $N_f/N_{of} = 1/2$ and T_C is approximately equal while in the extended Lieb lattice $N_f/N_{of} = 2/3$ and T_C is larger. However, in the twice-extended Lieb lattice, the flat-band ratio is also 1/2, but T_C is less than in the Lieb and connected lattices. This shows that the estimate $T_C \approx |U|N_f/(4N_{of})$ does not capture the full behavior of the critical temperature.

We note here that this mean-field result is similar to a lower bound for general (uniform pairing condition not assumed) bipartite lattices $|\langle \Delta^B \rangle| \geq |U|N_f/(2N_{of})$, where $|\langle \Delta^B \rangle|$ is the average of the order parameters of the larger sublattice at zero temperature.²⁷ We also confirm that for all of the bipartite lattices studied $|\langle \Delta^B \rangle|$ is indeed larger than the lower bound. While the lower bound is derived for bipartite lattices with half filled flat bands, we find that even for non-bipartite lattices (the stacked and twice extended two- and three-dimensional Lieb lattices) $|\langle \Delta^B \rangle|$ is larger than the lower bound. The two-dimensional twice extended and connected Lieb lattices do not even have exactly half-filled flat bands, and still the lower bound holds. Furthermore, the largest

$$\frac{|\langle \Delta^B \rangle| - |U|N_f/(2N_{of})}{|\langle \Delta^B \rangle|} \quad (5)$$

in bipartite lattices is 0.077 (Lieb lattice) and in non-bipartite lattices 0.155 (twice extended three-dimensional Lieb), which shows that the lower bound is close to $|\langle \Delta^B \rangle|$.

Figure 2 b) shows the square roots of the determinants of the superfluid weights and the BKT transition temperatures for the two-dimensional extensions. The superfluid weights vanish at the same temperatures as the order parameters, and thus, these critical temperatures of the superfluid weights also mirror the behavior of the flat-band ratio for the connected, extended and Lieb lattices. However, the BKT transition temperatures behave qualitatively differently. The original Lieb lattice has a larger T_{BKT} than the connected Lieb lattice, even though these have the same flat-band ratio. This shows that while the flat-band ratio succeeds at explaining the behavior of T_C for the Lieb, connected and extended lattices, it fails to fully explain the behavior of the BKT transition temperature.

C. Influence of the quantum metric

We also study different versions of the extended Lieb lattice shown in Fig.1 c). These different versions are called the diagonal, the x-directional and the decorated versions. All of these lattices have two degenerate flat bands at zero energy and three orbitals where these flat bands reside, resulting in a flat-band ratio of 2/3, which is larger than the 1/2 ratio of the original Lieb lattice. Thus, based on the results from the previous section, we could expect the critical temperatures of all the different versions to be larger than that of the original Lieb lattice. However, as seen from Fig.4 a), the x-directional and decorated versions have a nearly identical critical temperature to the original Lieb

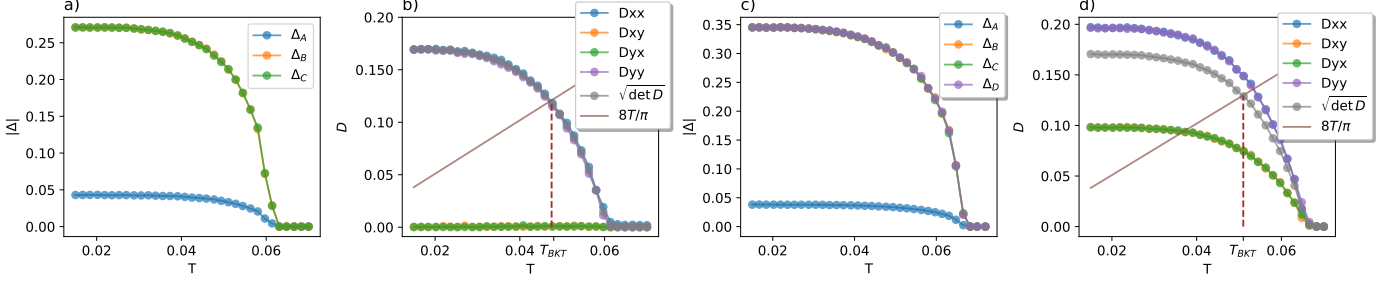


Figure 2. a) (c) Absolute values of order parameters as a function of temperature for the original Lieb lattice (two-dimensional extended Lieb). The order parameters of orbitals B and C (B, C and D) of the Lieb (two-dimensional extended Lieb) lattice are equal and thus visible as one line only. b) (d) the components of the superfluid weight and $\sqrt{\det D}$ for the original Lieb lattice (two-dimensional extended Lieb lattice). Both the diagonal components D_{xx} and D_{yy} are equal in the original Lieb and the extended Lieb lattices, and $D_{xy} = D_{yx}$.

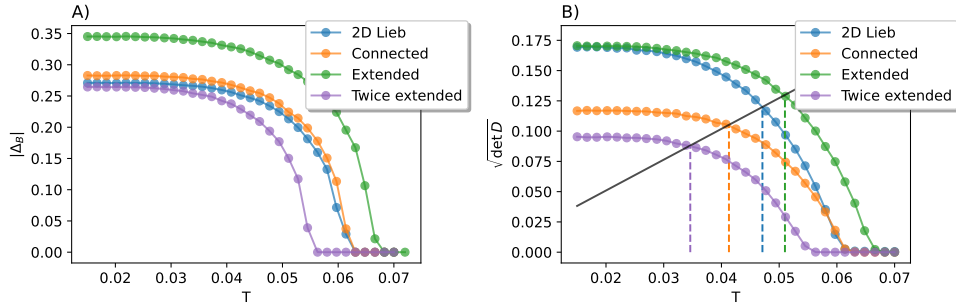


Figure 3. a) Absolute values of the order parameters as a function of temperature for the two-dimensional extended Lieb lattice (Fig. 1a)) with different interlayer hoppings, with the interaction strength $|U| = 1$ and the chemical potential $\mu = 0$. b) The square root of the determinant of the superfluid weight for the two-dimensional Lieb lattice, with interaction strength $U = 1$ and chemical potential $\mu = 0$.

lattice. Thus, in this case, the behavior in the critical temperatures for these versions fails to follow the flat-band ratio.

Figure 4 b) shows the square roots of the determinants of the superfluid weights and the BKT transition temperatures for the different versions. The flat-band ratio does not predict the behavior of T_{BKT} since all the different versions have different BKT temperatures while having the same flat-band ratio. Furthermore, T_{BKT} is larger for the original Lieb lattice than the decorated version, even though the decorated version has a larger flat-band ratio. These results show that while the flat-band ratio gives good predictions of the behavior of the critical temperature for some extensions of the Lieb lattice, it does not work for all of them. This suggests that there is some other key quantity affecting the behavior.

The quantum metric, known to determine many physical quantities of isolated flat bands, could be such a quantity. The quantum metric of a certain set of bands S is the real part of the quantum geometric tensor

$$\beta_{ij}(\mathbf{k}) = 2\text{Tr}P(\mathbf{k})\partial_i P(\mathbf{k})\partial_j P(\mathbf{k}), \quad (6)$$

where $P(\mathbf{k}) = \sum_{\beta \in S} |\beta_{\mathbf{k}}\rangle \langle \beta_{\mathbf{k}}|$ is the projector of the eigenstates to the Bloch states of the bands in the set S . In the

isolated flat-band limit the square root of the determinant of the zero temperature superfluid weight is proportional to the minimal quantum metric M^{\min} .^{14,15}

$$\sqrt{\det D_s} = \frac{4f(1-f)}{(2\pi)^{D-1}} \frac{N_f}{N_{of}} |U| \sqrt{\det M^{\min}}, \quad (7)$$

where D is the dimension, f is the filling factor of the flat bands, U the attractive interaction strength, and N_{of} (N_f) is the number of orbitals where the flat band states reside (degenerate flat bands). Here $\det M^{\min}$ denotes the determinant of the minimal quantum metric which is obtained by minimizing the trace of the integrated quantum metric

$$M_{ij} = \frac{1}{2\pi} \int_{\text{B.Z.}} d^2\mathbf{k} \text{Re}(\beta_{ij}(\mathbf{k})), \quad (8)$$

with reference to the positions of the orbitals in the unit cell, while tight-binding parameters are kept constant. In addition to the isolated flat-band limit, Eq. (7) assumes the presence of time-reversal symmetry and uniform pairing, i.e. that order parameters are equal in those orbitals where the flat band states reside.

Table I shows the predicted zero-temperature superfluid weights from the minimal quantum metrics for the different versions of the extended Lieb lattice shown in Fig. 1 c) with

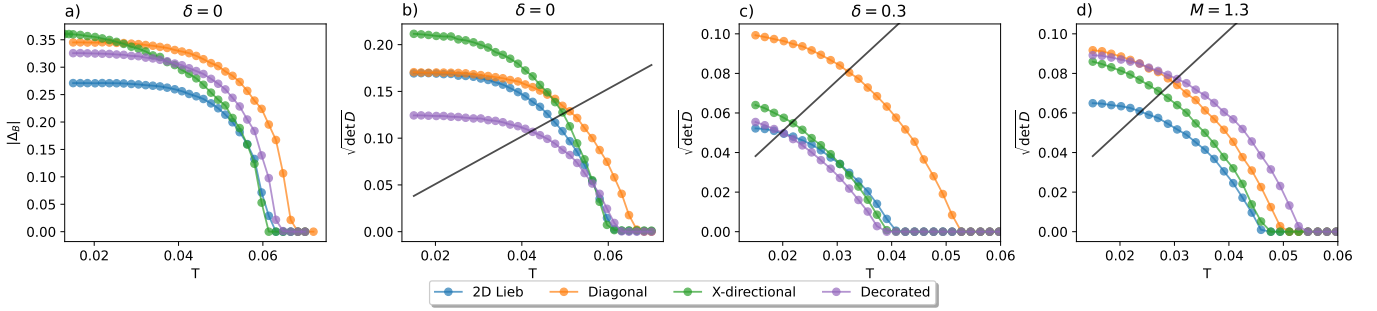


Figure 4. A-b) The absolute value of the order parameter $|\Delta_B|$ and the square root of the determinant of the superfluid weight as a function of temperature for the different versions of the extended Lieb lattice with $\delta = 0$. c) The square root of the determinant of the superfluid weight as a function of temperature for different versions of the extended Lieb with $\delta = 0.3$. d) The square root of the determinant of the superfluid weight as a function of temperature for different versions of the extended Lieb with the same determinant of the minimal quantum metric $\det M = 1.3$.

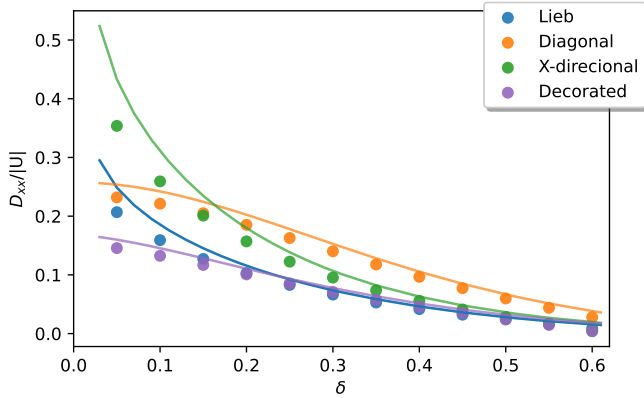


Figure 5. The D_{xx} component of the superfluid weight from DMFT calculations at $T = 0.003$ with $U = 0.3$ and from the minimal quantum metric prediction for the original Lieb and the different versions of the two-dimensional extended Lieb. The points give the DMFT superfluid weights and the lines give the predictions calculated using Eq. (7).

a hopping staggering $\delta = 0.3$. We have to use a non-zero δ since both the original Lieb lattice and the x-directional version (for $\delta = 0$) have a singular band touching point²⁸ where the quantum metric diverges. The staggering parameter δ increases the hoppings inside the unit cell and decreases them from one unit cell to another, which opens the band gap.

Fig. 4 c) shows $\sqrt{\det D}$ for the different versions of the extended and the original Lieb lattice with a staggering parameter $\delta = 0.3$. The critical temperatures of $\sqrt{\det D}$ behave similarly as in the $\delta = 0$ results, i.e., the diagonal version has a larger critical temperature while the other versions have approximately the same critical temperature. The zero temperature superfluid weights predicted from the quantum metric with $\delta = 0.3$, shown in Table I, overestimate the DMFT results (Fig. 4 C extrapolated to zero temperature) for all lattices, but correctly captures that the diagonal extended lattice has the highest zero-temperature D_s , followed by the x-directional extended, the decorated

Lieb lattice and finally the usual 2D Lieb lattice.

In Fig. 5, we compare the zero temperature superfluid predicted using Eq. (7) and the superfluid weight from DMFT calculations at $T = 0.003$ (which should be almost equal to the zero temperature superfluid weight). In the DMFT calculations, the interaction strength is $|U| = 0.3$ and the chemical potential is $\mu = 0$, corresponding to a half-filled flat band in all of the lattices. For the diagonal and decorated versions, the analytically predicted superfluid weight matches the DMFT one extremely well, while the prediction fails for the x-directional version and original Lieb lattice with small δ . This difference stems from differences in the band structures of these lattices shown in appendix IX A. The Lieb and the x-directional lattices have band touchings with $\delta = 0$, while the flat bands of the diagonal and decorated lattices are always separated.

In addition to the isolated flat band condition, Eq. (7) is derived assuming uniform pairing. From Fig. 2 c), we see that $|\Delta_A|$ is different from the other order parameters for the diagonal version of the extended Lieb lattice. This is, in fact, true for all the different extensions and the original Lieb lattice. The flat-band states reside on the B, C and D orbitals, which is why the different Δ_A does not affect the prediction much: we need uniform pairing at the orbitals where the flat-band states reside, whereas the order parameters at the other orbitals should be small in the isolated flat band limit. Interestingly, $|\Delta_C|$ differs from $|\Delta_B|$ and $|\Delta_D|$ in the x-directional version and $|\Delta_D|$ differs from $|\Delta_B|$ and $|\Delta_C|$ in the decorated version. Despite these differences in the order parameters, the scaled quantum metric prediction works well for the lattices when the band gap is sufficiently large. This indicates that the prediction works also when the uniform pairing condition is not perfectly met on the orbitals that have flat bands.

Appendix IX B, shows that when $|U| = 1$, the predicted superfluid weight overestimates the DMFT superfluid weight by a factor of $\frac{4}{3}$ but still has the same qualitative behavior as the DMFT superfluid weight. We also show in appendix IX B that the difference between the predicted superfluid weight and the DMFT one increases as a function of $|U|$ for the Lieb lattice and for all different ver-

Table I. Predicted zero-temperature superfluid weights for the different versions of the extended Lieb with $\delta = 0.3$. Here $\sqrt{\det D(0)}$ is calculated using Eq. (7).

Lattice	$\sqrt{\det D(0)}$ from quantum metric
original Lieb	0.073
Diagonal extended	0.130
X-directional extended	0.091
Decorated	0.077

sions of the extended Lieb lattice. These results show that while the mean-field prediction is quantitatively accurate only at small interaction strength (and exact at the limit of zero interaction strength), it can give surprisingly accurate qualitative predictions at higher interaction strengths. The match of the DMFT and the analytical prediction in Fig. 5 is, therefore, surprisingly good in many ways.

Fig.4 d) shows $\sqrt{\det D}$ for the different versions with such δ parameters that all the lattices have the same determinant of the minimal quantum metric of 1.3. The predicted zero-temperature superfluid weight is 0.121 for all three versions of the extended Lieb lattice and 0.091 for the original Lieb because of the smaller flat-band ratio. Now, the flat-band ratio prediction works better since $\det M^{\min}$ for the different versions is identical. We also find that $\sqrt{\det D}$ at higher temperatures is controlled by other factors besides the flat-band ratio and quantum metric. The critical temperatures T_D of $\sqrt{\det D}$ (and the BKT temperatures) of the different versions are clearly different, even though they have the same predicted zero-temperature superfluid weight. At higher temperatures, the dispersive bands play a bigger role, which could cause the difference between the different lattices since they have different dispersive bands.

From appendix IX A, we see that when $\det M^{\min}$ is 1.3, the diagonal and decorated versions have the largest band gaps, but also the largest almost flat parts in their dispersive bands. Both of these versions have larger T_D than the decorated x-directional Lieb lattice, which has a smaller band gap. This indicates that at higher temperatures, partly flat (or completely flat) bands away from the flat band(s) can enhance the superfluid weight. Yet, the decorated version has a larger T_D than the diagonal version while having less flat features in the dispersive bands. However, the band gap is significantly smaller for the decorated version, which in turn indicates that both the flat features of the dispersive band and its vicinity to the flat band(s) enhance superconductivity.

D. Three-dimensional extensions

Fig.1 c) shows how the two-dimensional Lieb lattice can be extended to three dimensions in a similar way as in Fig.1, a), i.e., the different extensions are made from the smaller sublattice. This preserves the flat band of the two-dimensional Lieb lattice. Once again, the (twice-) extended

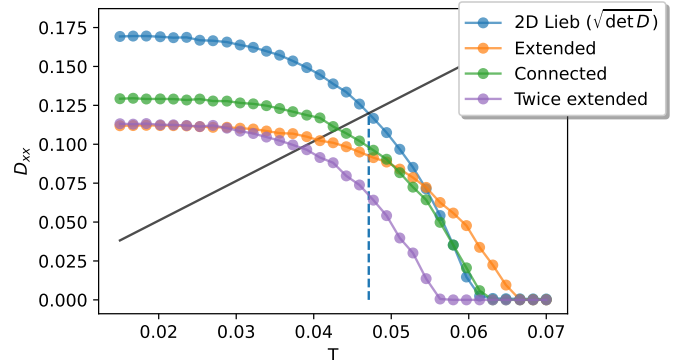


Figure 6. D_{xx} components of the superfluid weights of the different three-dimensional extensions and $\sqrt{\det D}$ of the two-dimensional Lieb lattice.

three-dimensional Lieb lattice has (two) one additional orbital(s) between the 2D planes. In the connected three-dimensional Lieb lattice, there is a straight hopping connection between the A sites. The flat-band ratios are the same in the three-dimensional extensions as in the two-dimensional ones, i.e., $2/3$ in the extended, whereas the twice-extended and connected lattices have the same flat-band ratio of $1/2$ as the Lieb lattice.

Fig.6 b) shows D_{xx} for the different three-dimensional extensions of the lattice and $\sqrt{\det D}$ for the original two-dimensional Lieb lattice. The temperatures at which the superfluid weight vanishes for the three-dimensional extensions follow the flat-band ratio similarly as in the two-dimensional extensions, i.e., the extended lattice has the largest critical temperature while connected has the second largest and twice extended the lowest. The temperature at which $\sqrt{\det D}$ vanishes for the two-dimensional Lieb equals the critical temperature of the connected extension. However, in the two-dimensional lattice, the real critical temperature of the superfluid weight is given by the BKT-transition temperature shown in Fig.6. In three dimensions, long-range order exists, and the real critical temperature of the superfluid weight is given by the temperature at which the superfluid weight vanishes. Thus, the critical temperature of superconductivity increases for all three-dimensional extensions compared to the two-dimensional Lieb lattice.

We have tested how important the fluctuations included in the DMFT method are by a comparison to a mean-field calculation, see appendix IX D. It turns out that a mean-field calculation at high temperatures produces not only quantitatively but also qualitatively different results: there seems to be an optimum for critical temperature in a quasi-two-dimensional regime. However, this does not appear in DMFT where the three-dimensional systems always lead to the highest T_c . This indicates that in predicting finite-temperature properties of flat-band superconducting systems, a beyond mean-field treatment is essential, while at $T = 0$, mean-field theory can give qualitatively accurate predictions as shown e.g. in Fig. 5.

E. Qualitative behavior of the superfluid weight and order parameters

Figure 7 shows that the superfluid weights of all the studied lattices, except the x-directional extension, have the same behavior as a function of temperature. In the two-dimensional cases the determinant of the superfluid seems to be in excellent agreement with the formula $\sqrt{\det D(T)} = \sqrt{\det D(0)}(1 - (T/T_c)^5)$ for all lattices except the x-directional for which a better matching analytical formula has a slightly smaller exponent of T/T_c . For the three-dimensional lattices Fig. 7 c) shows that the qualitative behavior of D_{xx} is in agreement with $D_{xx}(T) = D_{xx}(0)(1 - (T/T_c)^5)$.

We also find that in lattices with uniform pairing the order parameters of the orbitals in which the flat-band states reside are in excellent agreement with $\Delta(T) = \Delta(0)\sqrt{1 - (T/T_c)^5}$ (see appendix IX E). Thus, in lattices with UPC, the behavior of the superfluid weight is the same as the behavior of $\Delta(T)^2$. This relation is also present in Eq. (7) since in isolated flat bands with UPC the order parameter is given by $\Delta = N_f/N_{of}|U|\sqrt{f(1-f)}$ ¹⁵ and then Eq. (7) is given by

$$\sqrt{\det D_s} = \frac{4N_{of}\sqrt{\det M^{\min}}}{(2\pi)^{D-1}N_f|U|}\Delta^2. \quad (9)$$

Intriguingly, even when this relation only holds for isolated flat bands with UPC at zero temperature, our numerical results show that superfluid weight is proportional to Δ^2 also in nonisolated flat bands at non-zero temperatures.

Appendix IX E also shows the order parameters of the lattices without UPC, i.e. the x-directional and decorated extensions. In the x-directional extension $|\Delta_B|$ and $|\Delta_C|$ behave as $\Delta(T) = \Delta(0)\sqrt{1 - (T/T_c)^3}$, while Δ_C behaves as the order parameters of the lattices with UPC. Since $\sqrt{\det D_s}$ of the x-directional lattice matches better to an analytic formula with a smaller exponent of T/T_c , the superfluid weight could be connected to $\langle \Delta^F \rangle^2$ (the square of the average of the order parameters on the larger sublattice) rather than any single order parameter.

III. DISCUSSION

We investigated the critical temperature for superconductivity in several two- and three-dimensional extensions of the Lieb lattice with DMFT. While the superconducting properties for these extensions differ in various ways, we found that the flat-band ratio, i.e. the ratio of the number of flat bands at the Fermi energy to the total number of bands (or orbitals), plays a role in determining the critical temperature. For some of the models considered, the temperature at which the superconducting order parameters and the superfluid weight vanish increases when the flat-band ratio is increased. In a sense, this result can be expected, since the number of states at the Fermi energy is increased with the number of flat bands. However, other features of the band structure also seem to play a role at

high temperature: for instance, the diagonal extension of the two-dimensional Lieb lattice, which features partially flat dispersive bands, has an increased critical temperature compared to other versions of the extended Lieb lattice.

The importance of quantum geometry in the zero-temperature superfluid weight of flat bands is well-established and has been verified, for instance, by quantum Monte Carlo and DMFT computations.^{16-18,21} In this $T = 0$ limit, it is known that both the flat-band ratio and the minimal quantum metric play a role. Our results show that in this limit with small interaction strengths, the simple mean-field analytical result for the superfluid weight agrees with DMFT calculations even when the isolated flat band and uniform pairing conditions used in its derivation are poorly met. Furthermore, we find that with larger interaction strengths the analytical mean-field result agrees qualitatively with the DMFT calculations. A higher flat-band ratio can, in principle, result in a higher zero-temperature superfluid weight, but the quantum metric becomes zero when the ratio is brought to its maximal value of one (meaning that the system consists of only degenerate flat bands).

The zero-temperature superfluid weight typically only gives an upper bound for the critical temperature. The precise determination of T_{BKT} requires knowledge of the superfluid weight also at nonzero temperature. Our results suggest that the behavior of D_s at high temperatures is influenced by overall properties of the band structure: in addition to the flat-band ratio and the quantum metric of the flat band, the dispersion properties (or quantum metric) of the other bands also plays a role. Since a high flat-band ratio can both increase the zero-temperature superfluid weight and the temperature at which the superfluid weight vanishes, it can be expected to enhance T_{BKT} . Further studies could shed light on the behavior of D_s at intermediate temperatures, crucial for the determination of T_{BKT} . Our studies show that, at least in lattices with UPC, the superfluid weight at non-zero temperatures is determined by the zero-temperature superfluid weight and order parameter at the given temperature. At these temperatures, the behavior is probably dictated not only by the properties of the flat band(s) but also by the band dispersions, flat features and quantum geometric quantities of the nearby bands. Such studies could find out general properties favorable for high-temperature superconductivity.

Our results point to a potential method to design flat band systems with increased critical temperatures: the addition of orbitals resulting in an increased number of flat bands at the Fermi energy. The possible enhancement of the critical temperature is especially high if this extension adds a third dimension to a two-dimensional system, since reaching the BKT transition is no longer required. In our example case, this would be at the expense of the critical current at low temperatures since there the two-dimensional superfluid weight is larger.

Flat band models have been realized in ultracold atom experiments,²⁹⁻³² including the Lieb lattice.^{33,34} The high tunability of these systems makes them good candidates for the realization of lattice extensions. Moiré and other

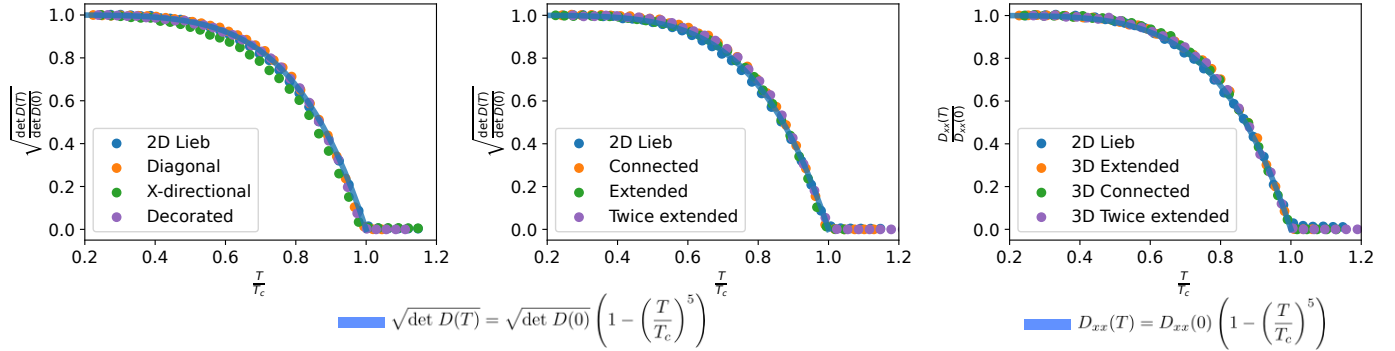


Figure 7. a) and b) Determinant of the superfluid weight scaled by the critical temperature and the zero temperature superfluid weight for all the two-dimensional modified Lieb lattices with $|U| = 1$. c) D_{xx} component of the superfluid weight scaled by the critical temperature and the zero temperature superfluid weight for the two-dimensional Lieb lattice and the tree-dimensional extensions with $|U| = 1$.

two-dimensional quantum materials^{4,5,11,35–37} offer unique possibilities for tuning the number of flat bands, orbitals in the (moiré) unit cell, and the quantum metric. One more interesting area of further study is stoichiometric three-dimensional flat band materials³⁸ where the number of relevant orbitals, flat bands and their quantum metrics can be obtained from ab-initio calculations and could help searches of materials with high critical temperatures and critical currents.

IV. METHODS

The usual mean-field treatment, where the interaction is replaced by an interaction with a mean-field, does not account for any of the fluctuations in the system. To include fluctuations at the local level, we use dynamical mean-field theory (DMFT), where the full lattice problem is mapped to an Anderson impurity model, in which the impurity is coupled to a bath of non-interacting particles.^{39–42} We use the unit cell of the lattice as an impurity and thus manage to account for fluctuations inside the unit cell. The essential approximation of DMFT is that the self-energy of the full lattice model is approximated by the self-energy of the impurity problem. This results in a self-energy that is local to each unit cell and varies only within unit cells but not between them, i.e., $\Sigma_{i,\alpha j,\beta}(i\omega_n) \approx \delta_{ij} \Sigma_{\alpha\beta}(i\omega_n)$, where i, j and α, β are the indices of the unit cells and orbitals respectively and $\omega_n = \pi(2n + 1)T$ are the fermionic Matsubara frequencies and T is the temperature.

Here we briefly describe how the DMFT works in the multi-band case described above. The full Green's function can be obtained from the non-interacting Green's function $\mathbf{G}_i^0(i\omega_n)$ and the self-energy with the Dyson equation

$$\mathbf{G}_i(i\omega_n) = \frac{1}{\mathbf{G}_i^0(i\omega_n)^{-1} - \Sigma_i(i\omega_n)}. \quad (10)$$

Since the self-energy is local to the unit cell, the non-local full Green's function is just the non-interacting Green's function, i.e., $\mathbf{G}_{i \neq 0}(i\omega_n) = \mathbf{G}_{i=0}^0(i\omega_n)$. After a Fourier

transformation, the Dyson equation for the local Green's function can be rewritten in momentum space as

$$\mathbf{G}_{loc}(i\omega_n) = \frac{1}{N_k} \sum_{\mathbf{k}} \frac{1}{\mathbf{G}_{\mathbf{k}}^0(i\omega_n)^{-1} - \Sigma(i\omega_n)}, \quad (11)$$

where N_k is the number of unit cells, i.e momentum points and $\mathbf{G}_{\mathbf{k}}^0(i\omega_n)^{-1}$ is the non-interacting Green's function in momentum space. The self-energy is a constant in momentum space because it is local to the unit cell in the real space. From this local Green's function and the self-energy, we can obtain the dynamical Weiss mean-field, which is essentially the non-interacting local Green's function

$$\Gamma(i\omega_n) = \frac{1}{\mathbf{G}_{loc}(i\omega_n)^{-1} + \Sigma(i\omega_n)}. \quad (12)$$

Then $\Gamma(i\omega_n)$ is used to define the Anderson impurity problem which we solve with the interaction expansion of continuous time Monte Carlo solver (CT-INT).^{43,44} We solve the self-energies and Green's functions self-consistently and then obtain the order parameters for each orbital from the anomalous components of the local Green's functions according to equation (4).

In two-dimensional systems, the transition to superconductivity occurs at the Berezinskii-Kosterlitz-Thouless (BKT) temperature T_{BKT} which can be obtained from the relation^{45–47}

$$T_{BKT} = \frac{\pi}{8} \sqrt{\det[D^s(T_{BKT})]}. \quad (13)$$

The superfluid weight is therefore a central quantity in this study. In DMFT, the superfluid weight can be obtained from the current density $\langle j_\mu \rangle$ induced by a constant vector potential A_ν with the linear response formula⁴⁸

$$\langle j_\mu \rangle = -D_{\mu\nu}^s A_\nu. \quad (14)$$

Here, the constant vector potential \mathbf{A} enters the hopping parameters by the usual Peierls substitution

$$\begin{aligned} t'_{i\alpha j\beta}(\mathbf{A}) &= e^{-i \int_{\mathbf{r}_j + \delta_\beta}^{\mathbf{r}_i + \delta_\alpha} \mathbf{A}(\mathbf{r}) d\mathbf{r}} t_{i\alpha j\beta} \\ &= e^{-i(\mathbf{r}_i + \delta_\alpha - \mathbf{r}_j - \delta_\beta) \cdot \mathbf{A}} t_{i\alpha j\beta}, \end{aligned} \quad (15)$$

where the \mathbf{r}_i and \mathbf{r}_j denote the positions of unit cells and δ_α and δ_β are the intra unit cell positions of the orbitals α and β . The current density operator at direction $\mu \in \{x, y, z\}$ can be obtained as the first derivative of the Hamiltonian with respect to a component of vector potential \mathbf{A} ^{14,49}

$$j_\mu = \frac{\partial H}{\partial \mathbf{A}_\mu} = \frac{\partial H^{kin}}{\partial \mathbf{A}_\mu} = \sum_{i,j} \frac{\partial t_{i,j}(\mathbf{A})}{\partial \mathbf{A}_\mu} c_i^\dagger c_j. \quad (16)$$

Then, the expectation value of the current operator can be calculated in the momentum space with⁴⁸

$$\langle j_\mu \rangle = \frac{1}{N} \sum_{\mathbf{k}} M_{\mathbf{k}} - \frac{1}{N\beta} \sum_{\mathbf{k}} \sum_n M_{\mathbf{k}} G_{\mathbf{k}}(i\omega_n), \quad (17)$$

where $M_{\mathbf{k}}$ is the matrix representation of the current operator in \mathbf{k} -space, $G_{\mathbf{k}}(i\omega_n)$ is the Green's function in mo-

mentum and frequency space and $N_{\mathbf{k}}$ is the number of \mathbf{k} points.

Now, the superfluid weight can be obtained using the following procedure: First, a constant small vector potential $\mathbf{A} = A_\nu$ in direction $\nu \in \{x, y, z\}$ is introduced to the hoppings with the Peierls substitution. Then the Green's functions of the system are calculated with the cluster-DMFT algorithm and the induced current in direction $\mu \in \{x, y, z\}$ is obtained with Eq.(17). Finally, the μ, ν component of the superfluid weight can be obtained from Eq. (14).

This procedure of calculating the superfluid weight does not work for every method and system, since a constant vector potential \mathbf{A} is usually gauge-equivalent to a zero vector potential, which does not produce any supercurrent.⁴⁸ However, at the DMFT level, we impose that the anomalous component of the self-energy, including the order parameters, is uniform in space, which breaks this gauge symmetry. Then the constant vector potential produces a phase twist on the order parameters and the off-diagonal anomalous components, which can not be gauged away.

* paivi.torma@aalto.fi

- ¹ Cao, Y. *et al.* Unconventional superconductivity in magic-angle graphene superlattices. *Nature* **556**, 43–50 (2018). URL <https://doi.org/10.1038/nature26160>.
- ² MacDonald, A. H. Bilayer graphene's wicked, twisted road. *Physics* **12**, 12 (2019). URL <https://physics.aps.org/articles/v12/12>.
- ³ Andrei, E. Y. & MacDonald, A. H. Graphene bilayers with a twist. *Nature Materials* **19**, 1265–1275 (2020). URL <https://www.nature.com/articles/s41563-020-00840-0>.
- ⁴ Andrei, E. Y. *et al.* The marvels of Moiré materials. *Nature Reviews Materials* **6**, 201–206 (2021). URL <https://doi.org/10.1038/s41578-021-00284-1>.
- ⁵ Bernevig, B. A. & Efetov, D. K. Twisted bilayer graphene's gallery of phases. *Physics Today* **77**, 38–44 (2024). URL <https://doi.org/10.1063/pt.jvsd.yhyd>.
- ⁶ Heikkilä, T., Kopnin, N. & Volovik, G. Flat bands in topological media. *JETP Letters* **94**, 233–239 (2011). URL <https://doi.org/10.1134/S0021364011150045>.
- ⁷ Shaginyan, V. & Khodel, V. Superfluidity in system with fermion condensate. *JETP Lett* **51**, 553 (1990).
- ⁸ Peotta, S. & Törmä, P. Superfluidity in topologically non-trivial flat bands. *Nature Communications* **6** (2015). URL <https://doi.org/10.1038/ncomms9944>.
- ⁹ Provost, J. P. & Vallee, G. Riemannian structure on manifolds of quantum states. *Communications in Mathematical Physics* **76**, 289–301 (1980). URL <https://doi.org/10.1007/BF02193559>.
- ¹⁰ Rossi, E. Quantum metric and correlated states in two-dimensional systems. *Current Opinion in Solid State and Materials Science* **25**, 100952 (2021). URL <https://doi.org/10.1016/j.cossms.2021.100952>.
- ¹¹ Törmä, P., Peotta, S. & Bernevig, B. A. Superconductivity, superfluidity and quantum geometry in twisted multilayer systems. *Nature Reviews Physics* **4**, 528–542 (2022). URL <https://doi.org/10.1038/s42254-022-00466-y>.
- ¹² Peotta, S., Huhtinen, K.-E. & Törmä, P. Quantum geometry in superfluidity and superconductivity. *ArXiv preprint* (2023). URL <https://doi.org/10.48550/arXiv.2308.08248>.

- ¹³ Tovmasyan, M., Peotta, S., Törmä, P. & Huber, S. D. Effective theory and emergent SU(2) symmetry in the flat bands of attractive Hubbard models. *Phys. Rev. B* **94**, 245149 (2016). URL <https://doi.org/10.1103/PhysRevB.94.245149>.
- ¹⁴ Huhtinen, K.-E., Herzog-Arbeitman, J., Chew, A., Bernevig, B. A. & Törmä, P. Revisiting flat band superconductivity: Dependence on minimal quantum metric and band touchings. *Physical Review B* **106** (2022). URL <https://doi.org/10.1103/PhysRevB.106.014518>.
- ¹⁵ Herzog-Arbeitman, J., Chew, A., Huhtinen, K.-E., Törmä, P. & Bernevig, B. A. Many-body superconductivity in topological flat bands. *arXiv preprint* (2022). URL <https://doi.org/10.48550/arXiv.2209.00007>.
- ¹⁶ Julku, A., Peotta, S., Vanhala, T. I., Kim, D.-H. & Törmä, P. Geometric origin of superfluidity in the Lieb-lattice flat band. *Phys. Rev. Lett.* **117**, 045303 (2016). URL <https://link.aps.org/doi/10.1103/PhysRevLett.117.045303>.
- ¹⁷ Peri, V., Song, Z.-D., Bernevig, B. A. & Huber, S. D. Fragile topology and flat-band superconductivity in the strong-coupling regime. *Phys. Rev. Lett.* **126**, 027002 (2021). URL <https://link.aps.org/doi/10.1103/PhysRevLett.126.027002>.
- ¹⁸ Herzog-Arbeitman, J., Peri, V., Schindler, F., Huber, S. D. & Bernevig, B. A. Superfluid weight bounds from symmetry and quantum geometry in flat bands. *Phys. Rev. Lett.* **128**, 087002 (2022). URL <https://link.aps.org/doi/10.1103/PhysRevLett.128.087002>.
- ¹⁹ Chan, S. M., Grémaud, B. & Batrouni, G. G. Pairing and superconductivity in quasi-one-dimensional flat-band systems: Creutz and sawtooth lattices. *Phys. Rev. B* **105**, 024502 (2022). URL <https://link.aps.org/doi/10.1103/PhysRevB.105.024502>.
- ²⁰ Chan, S. M., Grémaud, B. & Batrouni, G. G. Designer flat bands: Topology and enhancement of superconductivity. *Phys. Rev. B* **106**, 104514 (2022). URL <https://link.aps.org/doi/10.1103/PhysRevB.106.104514>.

- ²¹ Hofmann, J. S., Berg, E. & Chowdhury, D. Superconductivity, charge density wave, and supersolidity in flat bands with a tunable quantum metric. *Phys. Rev. Lett.* **130**, 226001 (2023). URL <https://link.aps.org/doi/10.1103/PhysRevLett.130.226001>.
- ²² Hofmann, J. S., Berg, E. & Chowdhury, D. Superconductivity, pseudogap, and phase separation in topological flat bands. *Phys. Rev. B* **102**, 201112 (2020). URL <https://link.aps.org/doi/10.1103/PhysRevB.102.201112>.
- ²³ Orso, G. & Singh, M. Pairs, trimers, and BCS-BEC crossover near a flat band: Sawtooth lattice. *Phys. Rev. B* **106**, 014504 (2022). URL <https://link.aps.org/doi/10.1103/PhysRevB.106.014504>.
- ²⁴ Iskin, M. Origin of flat-band superfluidity on the Mielke checkerboard lattice. *Phys. Rev. A* **99**, 053608 (2019). URL <https://link.aps.org/doi/10.1103/PhysRevA.99.053608>.
- ²⁵ Iskin, M. Effective-mass tensor of the two-body bound states and the quantum-metric tensor of the underlying Bloch states in multiband lattices. *Phys. Rev. A* **105**, 023312 (2022). URL <https://link.aps.org/doi/10.1103/PhysRevA.105.023312>.
- ²⁶ Herzog-Arbeitman, J. *et al.* Topological heavy Fermion principle for flat (narrow) bands with concentrated quantum geometry. *arXiv e-prints* (2024). URL <https://doi.org/10.48550/arXiv.2404.07253>.
- ²⁷ Bouzerar, G. & Thumin, M. Hidden symmetry of Bogoliubov de Gennes quasi-particle eigenstates and universal relations in flat band superconducting bipartite lattices. *Arxiv preprint* (2024). URL <https://doi.org/10.48550/arXiv.2310.06589>.
- ²⁸ Rhim, J.-W. & Yang, B.-J. Singular flat bands. *Advances in Physics: X* **6**, 1901606 (2021). URL <https://doi.org/10.1080/23746149.2021.1901606>.
- ²⁹ Jo, G.-B. *et al.* Ultracold atoms in a tunable optical kagome lattices. *Phys. Rev. Lett.* **108**, 045305 (2012). URL <https://doi.org/10.1103/PhysRevLett.108.045305>.
- ³⁰ Li, H. *et al.* Engineering topological chiral transport in a flat-band lattice of ultracold atoms. *arXiv e-prints* (2024). URL <https://doi.org/10.48550/arXiv.2401.03611>.
- ³¹ Li, H. *et al.* Aharonov-Bohm caging and inverse Anderson transition in ultracold atoms. *Phys. Rev. Lett.* **129**, 220403 (2022). URL <https://link.aps.org/doi/10.1103/PhysRevLett.129.220403>.
- ³² Leykam, D., Andreanov, A. & Flach, S. Artificial flat band systems: From lattice models to experiments. *Advances in Physics: X* **3**, 1473052 (2018). URL <https://doi.org/10.1080/23746149.2018.1473052>.
- ³³ Taie, S. *et al.* Coherent driving and freezing of bosonic matter wave in an optical Lieb lattice. *Sci. Adv.* **1**, 10 (2015). URL <https://doi.org/10.1126/sciadv.1500854>.
- ³⁴ Taie, S., Ichinose, T., Ozawa, H. & Takahashi, Y. Spatial adiabatic passage of massive quantum particles in an optical Lieb lattice. *Nature Communications* **11**, 257 (2020). URL <https://doi.org/10.1038/s41467-019-14165-3>.
- ³⁵ Andrei, E. Y. & MacDonald, A. H. Graphene bilayers with a twist. *Nature Materials* **19**, 1265–1275 (2020). URL <https://doi.org/10.1038/s41563-020-00840-0>.
- ³⁶ Wang, S., Song, J., Sun, M. & Cao, S. Emerging Characteristics and Properties of Moiré Materials. *Nanomaterials* **13** (2023). URL <https://www.mdpi.com/2079-4991/13/21/2881>.
- ³⁷ Tian, H. *et al.* Evidence for Dirac flat band superconductivity enabled by quantum geometry. *Nature* **614**, 440–444 (2023). URL <https://doi.org/10.1038/s41586-022-05576-2>.
- ³⁸ Regnault, N. *et al.* Catalogue of flat-band stoichiometric materials. *Nature* **603**, 824–828 (2022). URL <https://doi.org/10.1038/s41586-022-04519-1>.
- ³⁹ Maier, T., Jarrell, M., Pruschke, T. & Hettler, M. H. Quantum cluster theories. *Reviews of Modern Physics* **77**, 1027 (2005). URL <https://doi.org/10.1103/RevModPhys.77.1027>.
- ⁴⁰ Georges, A., Kotliar, G., Krauth, W. & Rozenberg, M. J. Dynamical mean-field theory of strongly correlated fermion systems and the limit of infinite dimensions. *Reviews of Modern Physics* **68**, 13 (1996). URL <https://doi.org/10.1103/RevModPhys.68.13>.
- ⁴¹ Hettler, M., Mukherjee, M., Jarrell, M. & Krishnamurthy, H. Dynamical cluster approximation: Nonlocal dynamics of correlated electron systems. *Physical Review B* **61**, 12739 (2000). URL <https://doi.org/10.1103/PhysRevB.61.12739>.
- ⁴² Kotliar, G. *et al.* Electronic structure calculations with dynamical mean-field theory. *Rev. Mod. Phys.* **78**, 865–951 (2006). URL <https://link.aps.org/doi/10.1103/RevModPhys.78.865>.
- ⁴³ Gull, E. *et al.* Continuous-time Monte Carlo methods for quantum impurity models. *Rev. Mod. Phys.* **83**, 349–404 (2011). URL <https://link.aps.org/doi/10.1103/RevModPhys.83.349>.
- ⁴⁴ Gubernatis, J., Kawashima, N. & Werner, P. *Quantum Monte Carlo Methods: Algorithms for Lattice Models* (Cambridge University Press, 2016).
- ⁴⁵ Berezinsky, V. L. Destruction of long range order in one-dimensional and two-dimensional systems having a continuous symmetry group. I. Classical systems. *Sov. Phys. JETP* **32**, 493–500 (1971).
- ⁴⁶ Kosterlitz, J. M. & Thouless, D. J. Ordering, metastability and phase transitions in two-dimensional systems. *Journal of Physics C: Solid State Physics* **6**, 1181–1203 (1973). URL <https://doi.org/10.1088/0022-3719/6/7/010>.
- ⁴⁷ Nelson, D. R. & Kosterlitz, J. M. Universal jump in the superfluid density of two-dimensional superfluids. *Phys. Rev. Lett.* **39**, 1201–1205 (1977). URL <https://link.aps.org/doi/10.1103/PhysRevLett.39.1201>.
- ⁴⁸ Liang, L. *et al.* Band geometry, Berry curvature, and superfluid weight. *Phys. Rev. B* **95**, 024515 (2017). URL <https://link.aps.org/doi/10.1103/PhysRevB.95.024515>.
- ⁴⁹ Vanhala, T. *Dynamical mean-field theory studies of superfluidity and topological phases in lattice models*. Ph.D. thesis, Aalto University, Finland (2018).

V. DATA AVAILABILITY

Data are available upon reasonable request.

VI. CODE AVAILABILITY

Code is available upon reasonable request.

VII. ACKNOWLEDGMENTS

The authors wish to acknowledge CSC – IT Center for Science, Finland, for computational resources. R.P. acknowledges financial support from the Fortum and Neste

Foundation. K.-E.H. is supported by an ETH Zurich Postdoctoral Fellowship. This work was supported by the Research Council of Finland (former Academy of Finland) under project number 339313 and by Jane and Aatos Erkko Foundation, Keele Foundation and Magnus Ehrn-

rooth Foundation as part of the SuperC collaboration.

VIII. AUTHOR CONTRIBUTIONS

PT initiated and supervised the project. RPS did the DMFT calculations. All authors discussed the results. RPS wrote the manuscript together with KEH and PT.

IX. APPENDIX

A. Band structures

The first and second rows of Fig. 8 show the band structures of the different versions and the original Lieb lattice with staggering parameters $\delta = 0$ and 0.3 , respectively. The original Lieb lattice and the x-directional version have band touchings at the high-symmetry point M when $\delta = 0$, which are opened with $\delta = 0.3$. The band structures of the diagonal and decorated versions have no band touchings even with $\delta = 0$. Furthermore, both dispersive bands of the diagonal Lieb lattice have a flat band portion along the high symmetry line from point M to point X . The last row of Fig. 8 shows that the diagonal and the decorated versions have the largest band gaps when the lattices have the same determinant of the minimal quantum metric of $\det M^{\min} = 1.3$. We also note that the band structures of the original Lieb and the x-directional version look similar in this case. Figure 9 shows the quantum metric distributed over the Brillouin zone in the different lattices. This helps us understand why certain lattices have higher superfluid weight than others. We note that the quantum metric can have a large effect when integrated over the Brillouin zone, even when there is a relatively large (compared to U) band gap to the next band(s).

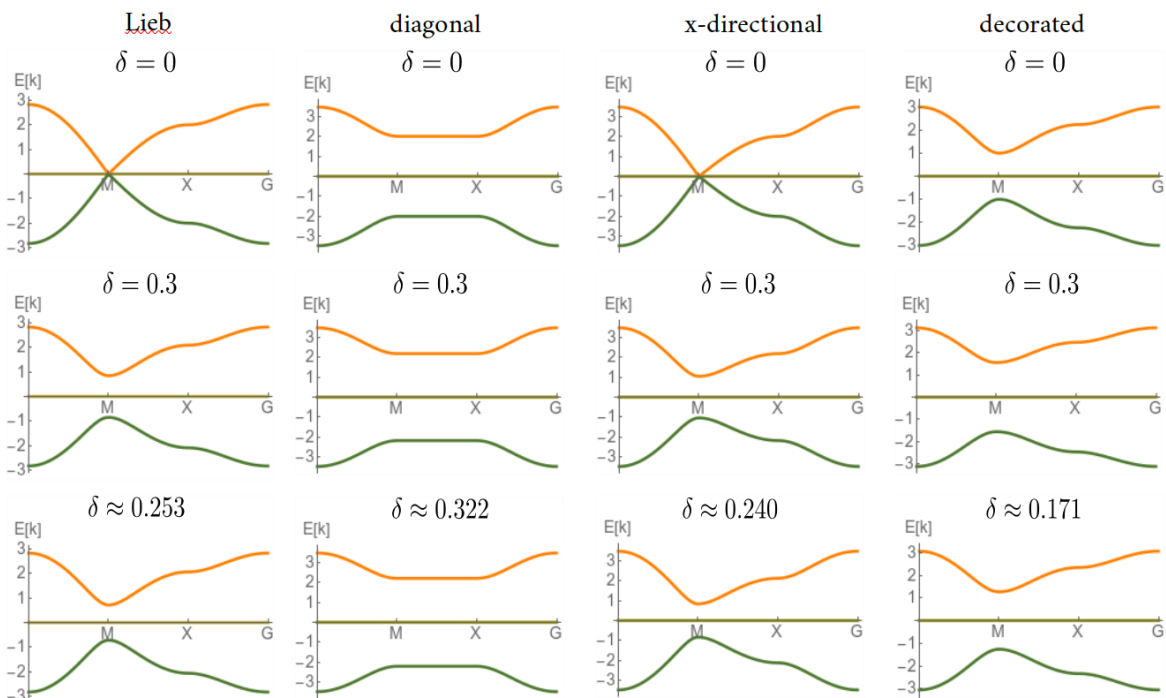


Figure 8. Band structures plotted along the high symmetry lines of the first Brillouin zone for the different versions of the extended Lieb lattice and the original Lieb lattice with $\delta = 0$ (first row), $\delta = 0.3$ (second row) and with such δ that $\det M^{\min} = 1.3$ (third row). The Lieb lattice has one flat band at zero energy for all δ , and the different versions all have two degenerate flat bands at zero energy.

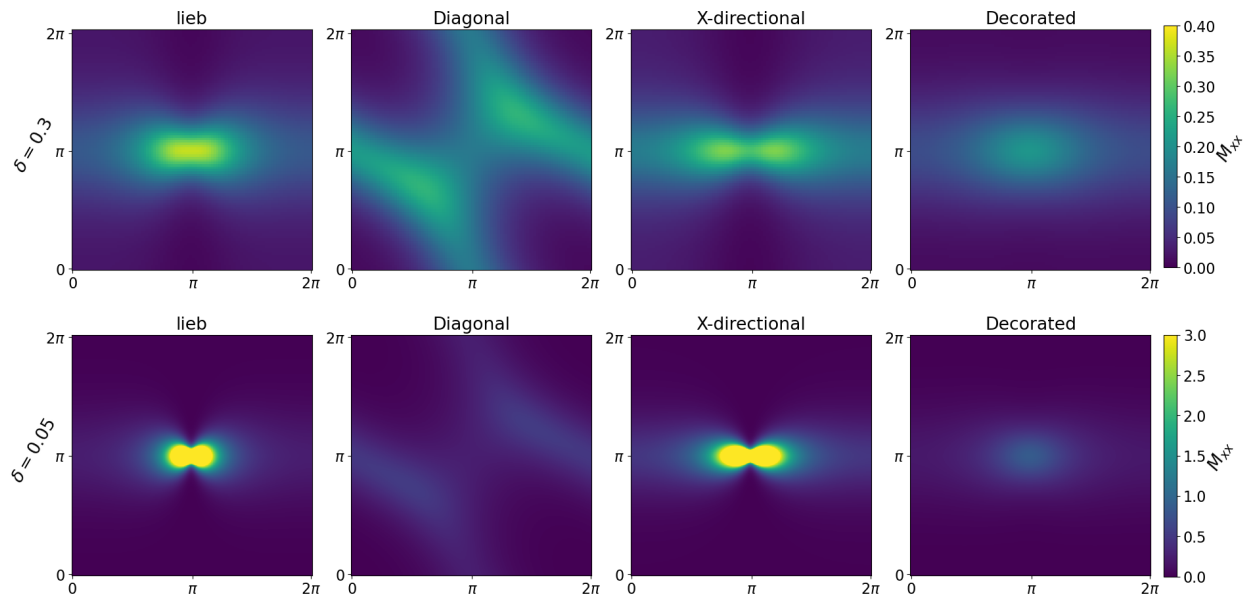


Figure 9. The minimal quantum metric (M_{xx}) of the flat band(s) in the first Brillouin zone for the different versions of the extended Lieb lattice with $\delta = 0.3$ (first row) and with $\delta = 0.05$ (second row).

B. Quantum metric prediction

Figure 10 a), shows the zero temperature superfluid predicted with Eq. (7) scaled by a factor of $\frac{3}{4}$ and the superfluid weight from DMFT calculations at $|U| = 1$ and $T = 0.01$ (which should be almost equal to the zero temperature superfluid weight). We find that the predicted superfluid weight overestimates the DMFT superfluid weight for all lattices. However, if the prediction obtained from the quantum metric is multiplied by a factor of $\frac{3}{4}$, the superfluid weights match well for all of the lattices when the band gap is sufficiently large. Figure 9 b) shows that the difference between D_{xx} predicted from the minimal quantum metric and DMFT superfluid weight at $T = 0.003$ increases as a function of $|U|$. These results indicate that when the interaction strength is increased Eq. (7) overestimates the superfluid weight compared to the DMFT results but succeeds to predict the qualitative behavior of D_{xx} as a function of δ .

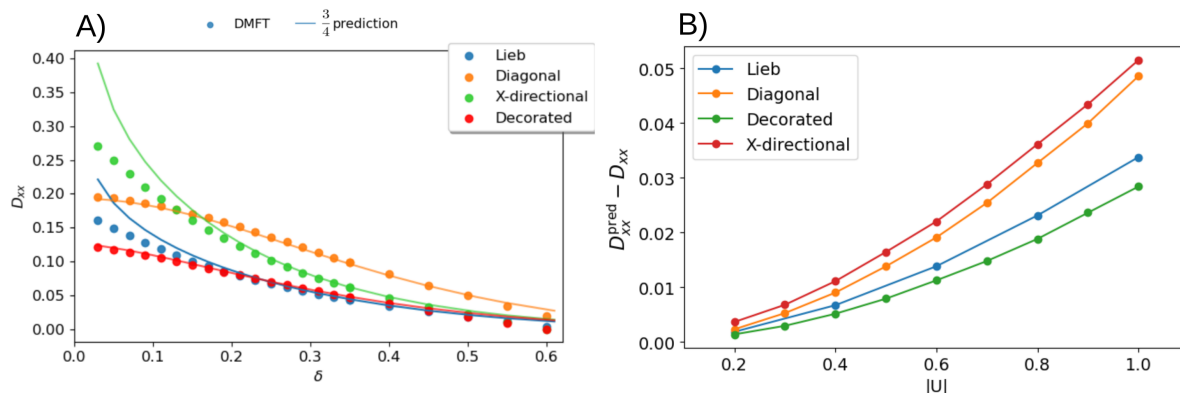


Figure 10. a) The D_{xx} component of the superfluid weight from DMFT calculations at $T = 0.01$ with $|U| = 1$ and from the minimal quantum metric prediction for the original Lieb and the different versions of the two-dimensional extended Lieb. The points give the DMFT superfluid weights and the lines give the predictions calculated using Eq. (7) scaled by a factor of $\frac{3}{4}$. b) Difference between the superfluid predicted from the minimal quantum metric at zero temperature and the DMFT superfluid weight at $T = 0.003$ as a function of the interaction strength $|U|$ with a staggering hopping $\delta = 0.2$.

C. Mean-field critical temperature

In this section, we compute the temperature T_{BCS} at which the order parameters vanish within mean-field theory in isolated flat bands with uniform pairing. We use a mean-field approximation of the interacting part of the Hubbard model (Eq. (1)),

$$U \sum_{i\alpha} c_{i\alpha\uparrow}^\dagger c_{i\alpha\uparrow} c_{i\alpha\downarrow}^\dagger c_{i\alpha\downarrow} \approx \sum_{i\alpha} \left[\Delta_\alpha c_{i\alpha\uparrow}^\dagger c_{i\alpha\downarrow}^\dagger + \text{H.c.} - |\Delta_{i\alpha}|^2/U \right], \quad (18)$$

where $\Delta_{i\alpha} = U \langle c_{i\alpha\downarrow} c_{i\alpha\uparrow} \rangle$ is the mean-field order parameter. Assuming that $\Delta_{i\alpha} = \Delta_\alpha$ is independent of the unit cell, the Hamiltonian in momentum space can be written in terms of the Bogoliubov-de-Gennes Hamiltonian H_{BdG} as $H = \sum_{\mathbf{k}} \mathbf{c}_{\mathbf{k}}^\dagger H_{\text{BdG}} \mathbf{c}_{\mathbf{k}}$, with

$$H_{\text{BdG}} = \begin{pmatrix} H_{\mathbf{k}} - \mu & \mathbf{\Delta} \\ \mathbf{\Delta}^\dagger & -H_{-\mathbf{k}}^* + \mu \end{pmatrix}, \quad (19)$$

$$\mathbf{c} = (c_{\mathbf{k}1\uparrow}, \dots, c_{\mathbf{k}N_o\uparrow}, c_{-\mathbf{k}1\downarrow}, \dots, c_{-\mathbf{k}N_o\downarrow})^T. \quad (20)$$

Here, $[H_{\mathbf{k}}]_{\alpha\beta} = \sum_i t_{0\alpha,i\beta} e^{i\mathbf{k}\cdot(r_{0\alpha}-r_{i\beta})}$, where $r_{i\beta}$ is the position of the lattice site $i\beta$, and $[\mathbf{\Delta}]_{\alpha\beta} = \Delta_\alpha \delta_{\alpha\beta}$. We assume now that the pairing is uniform throughout the lattice, i.e. $\Delta_\alpha = \Delta$, so that $\mathbf{\Delta} = \Delta \mathbf{1}$. We also assume time-reversal symmetry, implying $H_{\mathbf{k}} = H_{-\mathbf{k}}^*$, and take Δ real.

The non-interacting kinetic Hamiltonian $H_{\mathbf{k}}$ can be diagonalized as $H_{\mathbf{k}} = \mathcal{G}_{\mathbf{k}} \epsilon_{\mathbf{k}} \mathcal{G}_{\mathbf{k}}^\dagger$, where $[\epsilon_{\mathbf{k}}]_{m,n} = \epsilon_n(\mathbf{k}) \delta_{mn}$ contains the band dispersions and $[\mathcal{G}_{\mathbf{k}}]_{\alpha n} = \langle \alpha | n_{\mathbf{k}} \rangle$ the Bloch functions. We can thus rewrite H_{BdG} as

$$H_{\text{BdG}} = \begin{pmatrix} \mathcal{G}_{\mathbf{k}} & 0 \\ 0 & \mathcal{G}_{\mathbf{k}} \end{pmatrix} \begin{pmatrix} \epsilon_{\mathbf{k}} - \mu & \Delta \\ \Delta & -\epsilon_{\mathbf{k}} + \mu \end{pmatrix} \begin{pmatrix} \mathcal{G}_{\mathbf{k}}^\dagger & 0 \\ 0 & \mathcal{G}_{\mathbf{k}}^\dagger \end{pmatrix}. \quad (21)$$

The matrix H_{BdG} is now easily diagonalized, and has eigenvalues and vectors

$$E_n^\pm(\mathbf{k}) \equiv \pm E_n = \pm \sqrt{(\epsilon_n(\mathbf{k}) - \mu)^2 + \Delta^2}, \quad (22)$$

$$|\psi_n^+(\mathbf{k})\rangle = (u_n(\mathbf{k})|+\rangle + v_n(\mathbf{k})|-\rangle) \otimes |n_{\mathbf{k}}\rangle, \quad (23)$$

$$|\psi_n^-(\mathbf{k})\rangle = (-v_n(\mathbf{k})|+\rangle + u_n(\mathbf{k})|-\rangle) \otimes |n_{\mathbf{k}}\rangle, \quad (24)$$

$$(25)$$

where

$$u_m(\mathbf{k}) = \frac{1}{\sqrt{2}} \sqrt{1 + \frac{\epsilon_m(\mathbf{k}) - \mu}{E_m(\mathbf{k})}}, \quad v_m(\mathbf{k}) = \frac{1}{\sqrt{2}} \sqrt{1 - \frac{\epsilon_m(\mathbf{k}) - \mu}{E_m(\mathbf{k})}}. \quad (26)$$

The vectors $|\pm\rangle$ are the eigenvectors of the Pauli matrix σ_z corresponding to eigenvalues ± 1 . The full BdG Hamiltonian can thus be rewritten in a diagonal form $H = \sum_{\mathbf{k}} \gamma_{\mathbf{k}}^\dagger \mathbf{E}_{\mathbf{k}} \gamma_{\mathbf{k}} + C$, where C is a scalar which does not impact the following calculations and

$$\mathbf{E}_{\mathbf{k}} = \text{diag}(E_1^+(\mathbf{k}), \dots, E_{N_o}^+(\mathbf{k}), E_1^-(\mathbf{k}), \dots, E_{N_o}^-(\mathbf{k})), \quad (27)$$

$$\gamma_{\mathbf{k}} = (\gamma_{\mathbf{k}1+}, \dots, \gamma_{\mathbf{k}N_o+}, \gamma_{\mathbf{k}1-}, \dots, \gamma_{\mathbf{k}N_o-})^T, \quad (28)$$

$$c_{\mathbf{k}\alpha\uparrow} = \sum_n \langle \alpha | n_{\mathbf{k}} \rangle [u_n(\mathbf{k}) \gamma_{\mathbf{k}n+} - v_n(\mathbf{k}) \gamma_{\mathbf{k}n-}], \quad (29)$$

$$c_{-\mathbf{k}\alpha\downarrow}^\dagger = \sum_n \langle \alpha | n_{\mathbf{k}} \rangle [v_n(\mathbf{k}) \gamma_{\mathbf{k}n+} + u_n(\mathbf{k}) \gamma_{\mathbf{k}n-}]. \quad (30)$$

The order parameters can be solved from the gap equation

$$\Delta_\alpha = -\frac{|U|}{N_k} \sum_{\mathbf{k}} \langle c_{-\mathbf{k}\alpha\downarrow} c_{\mathbf{k}\alpha\uparrow} \rangle \quad (31)$$

$$= -\frac{|U|}{N_k} \sum_{\mathbf{k}} \sum_n |\langle \alpha | n_{\mathbf{k}} \rangle|^2 \left[u_n(\mathbf{k}) v_n(\mathbf{k}) \langle \gamma_{\mathbf{k}n+}^\dagger \gamma_{\mathbf{k}n+} \rangle - u_n(\mathbf{k}) v_n(\mathbf{k}) \langle \gamma_{\mathbf{k}n-}^\dagger \gamma_{\mathbf{k}n-} \rangle \right] \quad (32)$$

$$= \frac{|U|\Delta}{2N_k} \sum_{\mathbf{k}} \sum_n |\langle \alpha | n_{\mathbf{k}} \rangle|^2 \frac{\tanh(\beta E_n(\mathbf{k})/2)}{E_n(\mathbf{k})}. \quad (33)$$

Because we assume uniform pairing,

$$\Delta = \frac{1}{N_o} \sum_{\alpha} \Delta_{\alpha} = \frac{|U|\Delta}{2N_k N_o} \sum_{\mathbf{k}} \sum_n \frac{\tanh(\beta E_n(\mathbf{k})/2)}{E_n(\mathbf{k})}. \quad (34)$$

We now consider a set \mathcal{S} of N_f degenerate flat bands at energy $\epsilon_{\bar{n}}$. Then Eq. (34) becomes

$$1 = \frac{|U|N_f}{2N_o} \frac{\tanh\left(\beta\sqrt{(\epsilon_{\bar{n}} - \mu)^2 + \Delta^2}/2\right)}{\sqrt{(\epsilon_{\bar{n}} - \mu)^2 + \Delta^2}} + \frac{|U|}{2N_k N_o} \sum_{\mathbf{k}} \sum_{n \notin \mathcal{S}} \frac{\tanh(\beta E_n(\mathbf{k})/2)}{E_n(\mathbf{k})}. \quad (35)$$

Setting $\mu = \epsilon_{\bar{n}}$ and taking the limit $T \rightarrow T_{BCS}$ where $|\Delta| \rightarrow 0^+$ yields the critical temperature for a half-filled flat band

$$T_{BCS} = \frac{|U|N_f}{4N_o} + \frac{|U|}{2N_k N_o} \sum_{\mathbf{k}} \sum_{n \notin \mathcal{S}} \frac{\tanh(|\epsilon_n(\mathbf{k}) - \epsilon_{\bar{n}}|/(2T_{BCS}))}{|\epsilon_n(\mathbf{k}) - \epsilon_{\bar{n}}|/T_{BCS}}. \quad (36)$$

If the flat band is isolated so that $|\epsilon_n(\mathbf{k}) - \epsilon_{\bar{n}}|$ is very large at all momenta, the second term can be ignored and we obtain a critical temperature proportional to the flat-band ratio,

$$T_{BCS} \approx \frac{|U|N_f}{4N_o}. \quad (37)$$

This result can be generalized to models where the pairing is uniform only at those orbitals where the flat band states reside, and vanishingly small at other sites. In such cases, N_o should be replaced by the number of orbitals at which the flat band states reside, N_{of} . In the two-dimensional Lieb lattice, where the flat band states reside at the B/C sites, this gives an estimate of $|U|/8$ for T_{BCS} in the isolated band limit. In the three-dimensional once-extended extension, where the states of the two flat bands reside at the $B/C/D$ sites, the estimate for an isolated band is $|U|/6$. As can be seen from Fig. 11, this can be close to the mean-field T_{BCS} even when the bands are not isolated. The critical temperature obtained from DMFT is lower than the mean-field estimate.

One can make further estimates by assuming that the bands other than the flat bands of interest are (nearly) flat and separated from them by a small gap, i.e., $|\epsilon_n(\mathbf{k}) - \epsilon_{\bar{n}}| \simeq \delta$ where δ is a constant small compared to $|U|$. This allows to Taylor expand Equation (36) to second order in δ . This gives

$$T_{BCS} - \frac{|U|}{4} \simeq -\frac{|U|}{T_{BCS}^2} \frac{\delta^2 N_{other}}{48N_o}, \quad (38)$$

where N_{other} is the number of the bands other than the flat bands of interest. We see that for small δ , T_{BCS} will be

$$T_{BCS} \sim \frac{|U|}{4}, \quad (39)$$

which can be understood as the optimal case for the uniform pairing condition, since the flatness of the other bands maximizes the tanh-containing term in Equation (36). This is only the temperature at which the mean-field order parameters vanish, and does not take into account whether the superfluid weight is nonzero. In fact, in a system with only degenerate flat bands, the quantum metric of the degenerate band vanishes and so does the superfluid weight. However, once some of the bands are separated from the flat bands of interest by a gap δ , a nonzero quantum metric and therefore superfluid weight become possible.

Using $T_{BCS} \sim \frac{|U|}{4}$ on the right hand side of Equation (38) gives an estimate how much a finite small value of δ decreases T_{BCS} from the optimum $|U|/4$:

$$T_{BCS} \sim \frac{|U|}{4} - \frac{N_{other}}{3N_o} \frac{\delta^2}{|U|}. \quad (40)$$

D. Mean-field results

The decision to use DMFT calculations in this study was motivated by the quantum fluctuations that it manages to account for. One can also perform similar calculations with mean-field theory and obtain the order parameters and superfluid weights. However, in this case, all of the quantum fluctuations in the system are neglected. In this section, we investigate how mean-field results compare to the DMFT results. Fig.11 shows the absolute values of the order parameters

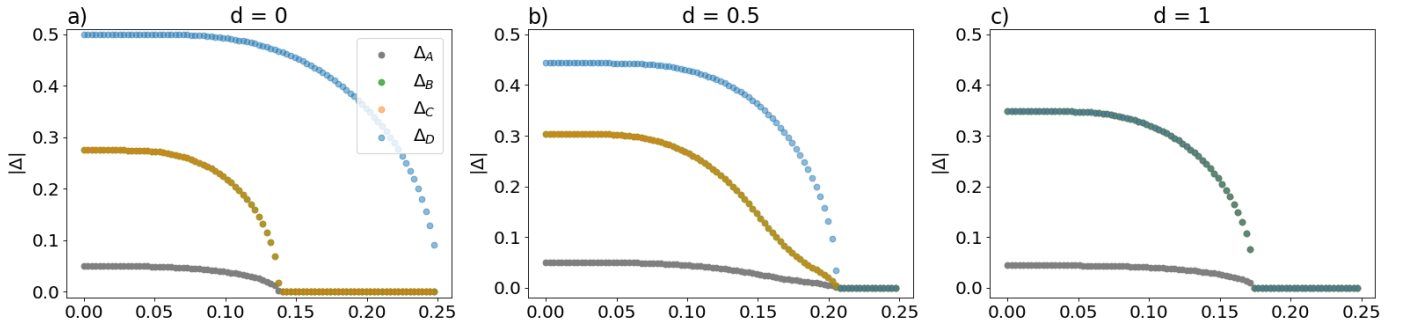


Figure 11. Absolute values of mean-field order parameters as a function of temperature for the extended three-dimensional Lieb lattice with different values of the interlayer hopping d . When $d = 0$ or $d = 0.5$, $|\Delta_B|$ and $|\Delta_C|$ are equal and with $d = 1$ all $|\Delta_B|$, $|\Delta_C|$ and $|\Delta_D|$ are equal.

for the three-dimensional extended Lieb lattice calculated with mean-field theory. We have introduced a hopping parameter d that gives the hopping strengths in z -direction. When $d = 0$, the system consisted of stacked two-dimensional Lieb lattices with disconnected orbitals between them and when $d = 1$, we have the three-dimensional extended Lieb lattice shown in Fig. 1 c). Using this parameter, we can tune our system continuously from the two-dimensional Lieb to the three-dimensional extended Lieb lattice.

The mean-field order parameters shown in Fig.11 are both qualitatively and quantitatively different from the DMFT order parameters. First, the critical temperatures of these order parameters are significantly larger than in the DMFT results. At the DMFT level, the local fluctuations are included, reducing the critical temperatures. More interesting is that now the critical temperature of the order parameters with $d = 0.5$ is larger than with $d = 0$ or with $d = 1$, which indicates that this critical temperature is maximized in the quasi-2D regime, i.e., with d between 0 and 1. In the DMFT context, the critical temperature of the three-dimensional extended Lieb lattice with $d = 0.5$ was between the $d = 0$ and $d = 1$ critical temperatures and the critical temperature was maximized with $d = 1$. Thus, the mean-field behavior is clearly different from that of the DMFT results.

This behavior can be explained by the order parameter of the disconnected D site (Δ_D) in the $d = 0$ case. When $d = 0$, Δ_D is zero in the DMFT results but nonzero (and large) in the mean-field results. This shows that in the absence of fluctuations, i.e., at the mean-field level, Cooper pairing is possible in the disconnected D orbitals. Furthermore, Δ_D has a larger critical temperature than other orbitals when $d = 0$. For small but non-zero d these strong Cooper pairs in the D sites with large critical temperatures seem to enhance Cooper pairing in other orbitals, which raises the critical temperatures of these orbitals. This results in the critical temperature being maximized in the quasi-2D regime. However, this large order parameter is only an artifact of the mean-field approximation and not physical since it is not present in the more precise DMFT calculations. Thus, DMFT calculations are needed to produce reliable results for the different extensions.

It was also confirmed that even in real-space DMFT results, the order parameter of the orbital D is zero when $d = 0$. In the real-space DMFT, each orbital is mapped to its own impurity problem, while in the DMFT method used earlier, the impurity was the entire unit cell. This real-space DMFT includes the fluctuations inside the orbitals, while the so-called cluster DMFT also includes fluctuations between different orbitals in the unit cell. However, also these intra-orbital fluctuations can break the Cooper pairing in the disconnected D sites, producing zero Δ_D when $d = 0$.

E. Qualitative behavior of the order parameters

Fig. 12 a) shows that for all of the studied lattices with UPC, the order parameters of the orbitals at which the flat-band states reside agree extremely well with $|\Delta(T)| = |\Delta(0)|\sqrt{1 - (T/T_c)^5}$. Fig. 12 b) shows the order parameters for the x -directional version which does not have UPC. While $|\Delta_C|$ still behaves as the order parameters of the lattices with UPC, $|\Delta_B|$ and $|\Delta_D|$ behave according to $|\Delta(T)| = |\Delta(0)|\sqrt{1 - (T/T_c)^3}$. Similar behavior is also seen for the decorated extension in Fig. 12 c), where $|\Delta_D|$ behaves as $|\Delta(T)| = |\Delta(0)|\sqrt{1 - (T/T_c)^3}$ while $|\Delta_B|$ and $|\Delta_C|$ behave as $|\Delta(T)| = |\Delta(0)|\sqrt{1 - (T/T_c)^5}$.

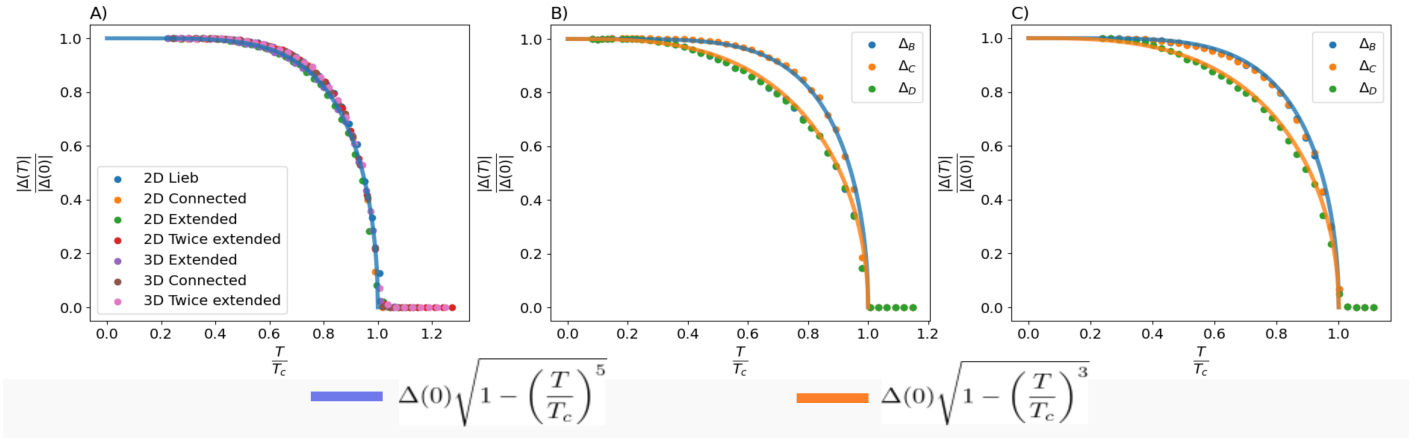


Figure 12. a) The scaled order parameter of the orbitals at which flat-band states reside for all the lattices with UPC with $|U| = 1$. b) (c) The scaled order parameters of the x-directional (decorated) versions with $|U| = 1$.